ARTICLE

# Humidity-Enhanced Thermally Tunable TiO₂/SiO₂ Bragg Stacks

Ida Pavlichenko,[†,‡,⊥] Armin T. Exner,[§,⊥] Markus Guehl,[§] Paolo Lugli,[§] Giuseppe Scarpa,[§] and Bettina V. Lotsch[*,†,‡]

[†]Max Planck Institute for Solid State Research, Heisenbergstrasse 1, 70569 Stuttgart, Germany

[‡]Department of Chemistry and Center for Nanoscience (CeNS), Ludwig Maximilian University of Munich (LMU), Butenandtstrasse 5-13 (D), 81377 Munich, Germany

[§]Institute for Nanoelectronics, Technical University of Munich, Arcisstrasse 21, 80333 Munich, Germany

Ⓢ *Supporting Information*

ABSTRACT:
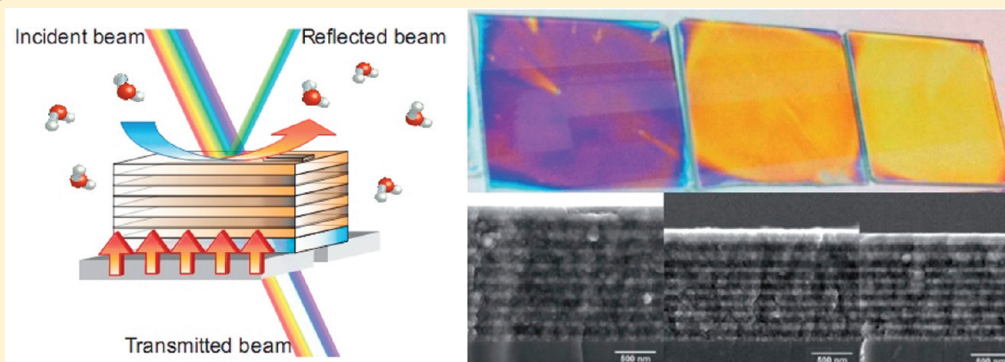
Tunable, stimuli-responsive photonic crystals (PCs) have developed into a fast growing, interdisciplinary research field attracting attention from various scientific communities, such as photonics, sensing, and materials chemistry. Here, we propose a thermally tunable and environmentally responsive optical filter derived from nanoparticle-based TiO₂/SiO₂ one-dimensional photonic crystals, christened Bragg stacks (BSs). Photonic crystals with textural mesoporosity were obtained by bottom-up assembly based on sequential spin-coating suspensions of TiO₂ and SiO₂ nanoparticles on glass substrates. The mechanism of the BS thermal tunability is based on the thermo-optic effect, i.e., dependence of the refractive index on temperature. Notably, the optical response of the BS to temperature can be significantly enhanced by varying the relative humidity of the environment. Thus, the magnitude of the spectral shift increases more than fourfold from 4.4 to 21.9 nm with a change in relative humidity from 25% to 55% in the temperature range between 15 and 60 °C. Thus, humidity-enhanced thermal tuning causes shifts of the transmission spectra by up to −1.66 nm K⁻¹. The simulations of the wavelength shift based on the measurement of the effective thermo-optic coefficient of the individual TiO₂ and SiO₂ layers at ambient conditions closely correspond to the experimental values. Owing to their high inherent porosities and ease of fabrication, nanoparticle-based BSs offer a great potential for the development of sensitive, label-free photonic crystal temperature and humidity sensors.

■ INTRODUCTION

Photonic crystal (PC) research has witnessed rapid progress over the past years, materializing in the development of photonic crystal building blocks for various optical systems, for example, in fiber-optic communication networks as wavelength-division and add−drop multiplexers, microelectro-mechanical systems (MEMS), infrared spectrometers, and color displays.[1−3] "Smart" photonic crystals further extend the range of applications toward environmentally responsive and, hence, *tunable* optical filters, as they are able to dynamically respond to external stimuli through optical thickness changes. An emerging area of applications of stimuli-responsive PCs is the development of label-free biological, chemical, and physical sensors.[4,5] The sensing approach is based on the utilization of PCs as tunable optical filters capable of

changing their refractive properties when in contact with an analyte of interest or when exposed to external stimuli such as electric and magnetic fields, pH, etc. Thermo- and hygroresponsive PCs are of particular interest because of the increasing demand for compact, low-cost, and label-free temperature and humidity sensors.

1D PCs, christened Bragg stacks (BSs), are interference-based optical multilayer structures consisting of a periodic stack of layers of two different materials featuring high and low refractive indices (*n*), respectively. The periodicity of the dielectric lattice
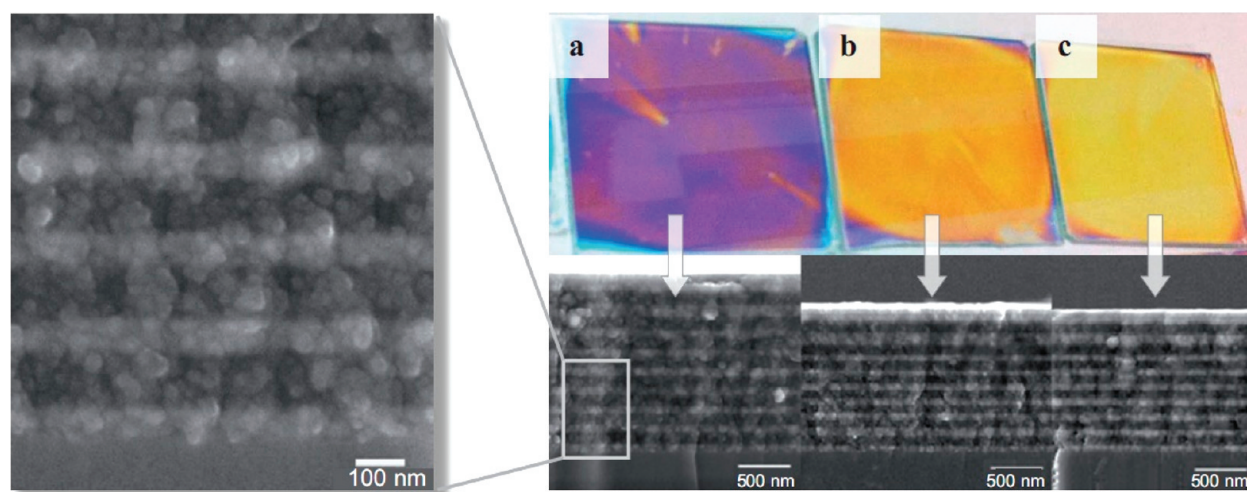
Figure 1. SEM images showing the relationship between the color of the TiO_2/SiO_2 Bragg stacks and the thickness of the layers spin-coated at (a) 2500, (b) 4500, and (c) 5500 rpm with an acceleration of 1500 rpm s^{-1}. Left: Magnification of the cross-section image in (a) to demonstrate the porous morphology of the layers.

of the multilayer structure creates a periodic potential for photons in one dimension, such that photons with particular energies cannot propagate within the PC. The resulting photonic band gap, called stop band, gives rise to photons being reflected in a particular wavelength range, resulting in "structural color" as opposed to color originating from light absorption by chromophores.[6] The central wavelength of the stop band can be calculated by the Bragg−Snell law for normal incidence (eq 1):

$$m\lambda = 2(n_H h_H + n_L h_L) \quad (1)$$

where m is the diffraction order and n_H, n_L, h_H, and h_L are the respective refractive indices and thicknesses of the high- (H) and low- (L) refractive index (RI) materials. Therefore, the position of the stop band can be modulated by varying the optical thickness (the product of RI and physical thickness) of the layers.[7]

One possible mechanism of color tuning is based on the thermo-optic effect (TOE), i.e., the dependence of the RI of a material on temperature. Titanium dioxide is an excellent optical coating material due to its high transparency above 350 nm and high RI (1.8−2.5). The thermo-optic coefficient (TOC) of titanium dioxide measured for coatings deposited by electron beam physical vapor deposition is negative and equal to -1.77×10^{-4} K^{-1} between 18 and 120 °C and -3.04×10^{-4} K^{-1} between 220 and 325 °C at 800 nm.[8] Xie et al.[9] compared the TOC of titanium dioxide films obtained by magnetron sputtering. The TOC of nonannealed films was found to be -1.21×10^{-4} K^{-1}, while values around -2.14×10^{-4} K^{-1} were reported for an annealed sample in the temperature range 31−105 °C at 632 nm. Measurements of TOCs of sol−gel-derived TiO_2 films have not yet been reported. In contrast, the thermo-optic coefficient of silicon dioxide is positive and ranges between 0.88×10^{-5} and 1.34×10^{-5} K^{-1}.[10] A change in RI due to the change of thickness is negligible since the thermal expansion coefficient (TEC) for both materials is on the order of 10^{-6} K^{-1}. The tuning mechanism based on the TOE has already been demonstrated on optical filters produced mainly by expensive deposition techniques such as sputtering, electron beam

evaporation, or plasma-enhanced chemical vapor deposition. The tuning efficiency of a single amorphous Si cavity arranged between Si_3N_4/SiO_2 distributed Bragg reflectors (DBRs) was measured[11] to be 0.05 nm K^{-1}, whereas that of a polycrystalline (poly-)Si cavity in poly-Si/SiO$_2$ DBRs[12] was reported to be 0.07 nm K^{-1}. A similar approach demonstrated thermal tunability of the emission of conjugated polymers embedded in a microcavity between DBRs deposited by reactive electron beam evaporation.[13] The photoluminescence spectra of the polymers inside the cavity were tuned with an efficiency of -0.2 nm K^{-1}. A wavelength shift of 0.01 nm K^{-1} was verified for external-cavity DBR laser with a silica fiber Bragg grating.[14] The performance of thin-film optical filters in the presence of humid atmosphere has been a subject of interest in several studies.[15−21] The principal objective of these investigations was to determine the influence of water vapor exposure on the stability of the spectral characteristics of band-pass filters. Still, the effect of moisture adsorption and desorption as a function of temperature was not hitherto examined as a feasible mechanism for enhancement of the tuning efficiency of the thin film coatings.

The sol−gel method affords a relatively simple, fast, and low-cost synthetic pathway to produce nanoparticles for the assembly of 1D PCs with high optical and structural quality by spin-coating.[22,23] An intrinsic property of nanoparticle-based 1D PCs is the high porosity of the constituent layers, giving rise to versatile and multifunctional multilayer architectures which can be fabricated in a straightforward manner. In particular, Bragg stacks built from TiO_2/SiO_2 nanoparticle multilayers have already demonstrated their great potential in chemical vapor and liquid detection.[24−30] An additional benefit of these systems stems from their self-cleaning properties provided by the photo-activity of TiO_2 particles under UV irradiation and the porosity-driven superwetting behavior ensuring the superhydrophilic properties of such BSs.[31] However, the impact of ambient conditions such as temperature and humidity on their optical response remains elusive. In this work we present a thermo- and hygrotunable optical filter and specifically point out the effect of ubiquitous humidity on the thermal response of photonic crystals. To the best of our knowledge, cross-correlation effects between temperature and ambient humidity in tunable 1D PCs

Table 1. Dependence of the Thickness of the Layers in the Bragg Stack on the Rotation Speed during Spin-Coating

rotation speed (rpm)[a]	TiO₂ layer thickness (nm)[b]	SiO₂ layer thickness (nm)
2500	75 ± 3	118 ± 3
4500	60 ± 3	93 ± 2
5500	56 ± 3	80 ± 2

[a] Acceleration 1500 rpm s⁻¹. [b] Note that the thickness values are given after calcination of the layers for 30 min at 350 °C.
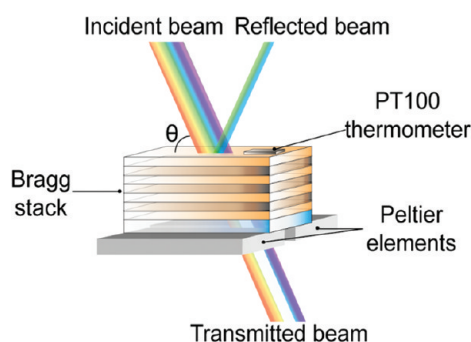

Figure 2. Schematic drawing of the experimental setup. The Bragg stack is deposited on a transparent glass substrate placed on thermoelectric heaters. The PT100 thermometer tracks the actual temperature. The Bragg stack acts like an optical filter for the incident beam resulting in the observation of the photonic stop band. In our experiment the beam hits the surface of the Bragg stack at an angle of $\theta = 90°$ (i.e., orthogonal incidence).

have been largely neglected so far. We propose that exploiting them may offer great potential for the development of highly sensitive PC optical sensors featuring a humidity-enhanced temperature response and shed light on the fundamental aspects of the water-adsorption-induced colorimetric behavior of porous multilayer systems.

■ RESULTS AND DISCUSSION

Bragg Stack Assembly and Characterization. Bragg stacks were assembled by sequential spin-coating of stable colloidal suspensions of TiO₂ and SiO₂ nanoparticles. In order to enhance the layer stability and mutual layer adhesion, calcination steps at 350 °C for 30 min were added after depositing each individual layer. The scanning electron microscopy cross-sectional images of the Bragg stacks are shown in Figure 1. The layers of TiO₂ and SiO₂ can be identified as bright (higher electron density) and dark stripes, respectively. Different "structural" colors of the PCs shown arise from variation of the lattice parameters resulting from different spin-coating rotation speeds. Information about the thickness of the layers can be derived from spectroscopic ellipsometry by fitting the experimentally obtained data to a Cauchy dispersion equation (see Table 1). An important observation is that the layers constituting the Bragg stack are porous. The porosity calculated by spectroscopic ellipsometry using the Lorentz–Lorenz equation and toluene as adsorptive is 10% for TiO₂ and 25% for SiO₂.[32,33] The degree of porosity can be kept constant by strict control of the nanoparticle synthesis and calcination conditions.

We confirmed the crystalline nature of the TiO₂ nanoparticles calcined at 350 °C by powder X-ray diffraction, which clearly
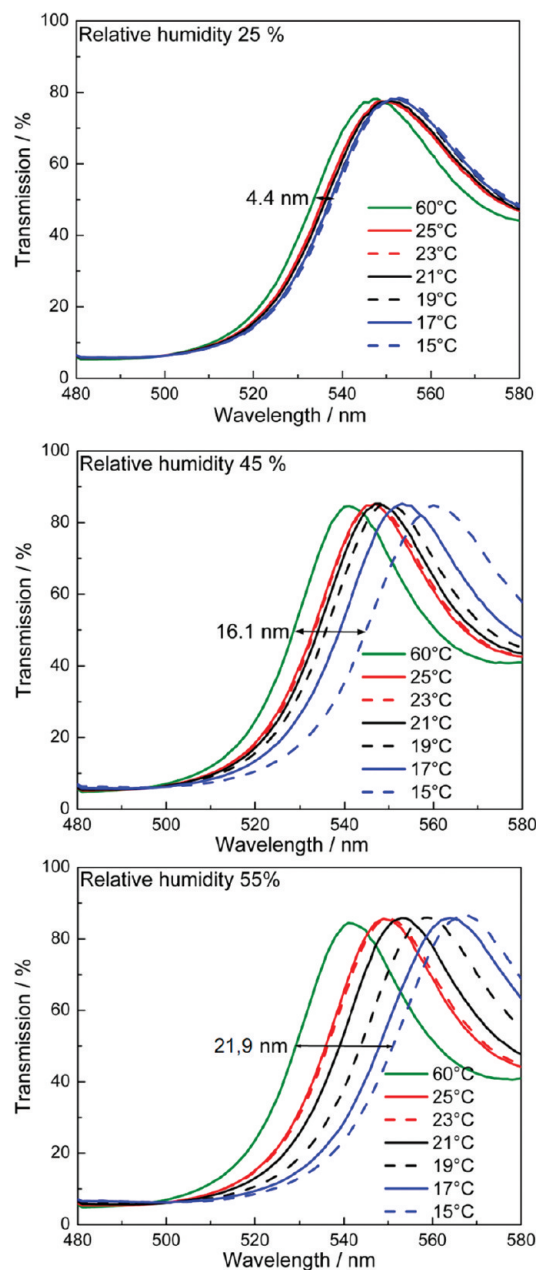

Figure 3. Transmission spectra of the TiO₂/SiO₂ BS shown in Figure 1b, demonstrating the blue shift in the temperature range between 15 and 60 °C and at various relative humidities (RH): 25%, 45%, and 55%. The relative humidity was measured at 20 °C. Spectra between 25 and 60 °C are omitted for clarity. The black double arrow indicates the magnitude of the shift in toto.

shows the signature of the anatase polymorph (Figure S1, Supporting Information). The crystallite size of the TiO₂ nanoparticles derived from the Scherrer equation is around 6 nm, while dynamic light scattering (DLS) gives the number size distribution of the values for the hydrodynamic diameter between 7 and 15 nm (Figure S2). The hydrodynamic diameter derived for the SiO₂ particles ranges between 6 and 10 nm.

Thermo-optical Behavior. Figure 2 depicts a simplified scheme of the experimental setup and the general principle of temperature sensing with 1D PCs. To realize the temperature tuning, the BS, deposited on a transparent glass substrate, was
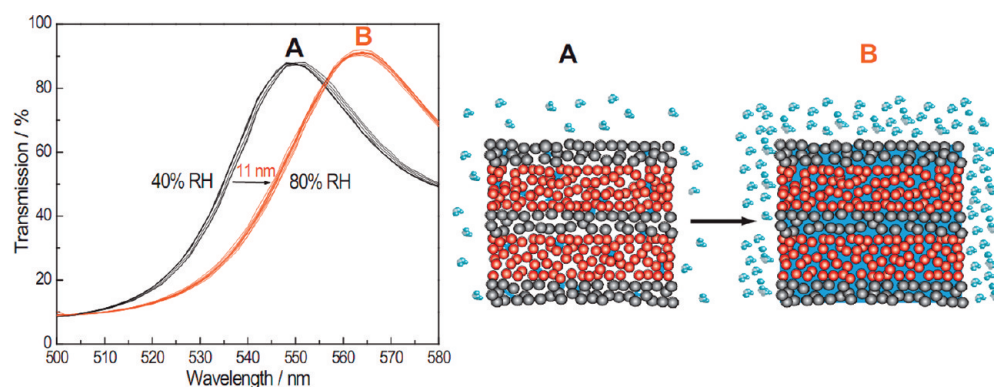
Figure 4. Effect of a change in humidity on the Bragg stack stop band position at constant temperature. Several cycles are shown to demonstrate the reversibility of the water adsorption and desorption. The black arrow indicates 11 nm red shift upon increasing RH from 40% (A) to 80% (B). The scheme on the left demonstrates the increase of the water content in the BS pore network upon augmenting the RH, which results in the enlargement of the effective refractive index of the layers.

placed on thermoelectric heaters and connected to a resistance thermometer (Pt100) capable of tracking the actual temperature. The BS was positioned between the monochromator and the detector such that the incident beam was normal to the surface of the sample (divergence angle $\approx 3°$). Using this setup, the BS modifies the spectrum of the incident light as a function of temperature by acting as a thermoresponsive optical filter.

We performed the thermo-optic experiments with the BS presented in Figure 1b, as it exhibited the highest optical quality and homogeneity. Transmission spectra were measured in the temperature region between 15 and 60 °C with steps of 2 °C between 15 and 25 °C, and with steps of 5 °C between 25 and 60 °C (Figure 3). The BS was thermally equilibrated for 1 min before taking the measurement. The transmission of the substrate (98.5%) did not change during heating. For a clear representation only the red edge of the photonic stop band between 480 and 580 nm is shown. In all experiments, we consistently observed a blue shift of the transmission spectra during heating, which was confirmed by taking measurements at different spots on the BS. The blue shift is fully consistent with the large, yet negative TOC of TiO_2 and the small positive TOC of SiO_2. Notably, however, the shifts observed were significantly larger than those expected to be induced by the thermo-optic effect with the literature values of TOCs reported for TiO_2 and SiO_2 and prognosticated to have less than 2 nm shift between 15 and 60 °C. In order to explore the nature of the observed enhancement effect further, the experiments were performed under ambient conditions (RT, 20 °C) with varying relative humidities (RH) of 25%, 45%, or 55%. Figure 3 outlines the impact of ambient RH on the temperature response of the BS. At a RH of 25%, the shift amounts to 4.4 ± 0.1 nm in the temperature range from 15 to 60 °C. For a RH of 45% the shift equals 16.1 ± 0.6 nm within the same temperature range. At a RH of 55%, a shift of 21.9 ± 1.7 nm is observed. The inherent porosity of nanoparticle Bragg stacks due to interparticle voids provides a quick response pathway to the humidity of ambient air. The change in temperature induces two parallel effects: a change of the refractive indices of the TiO_2 and SiO_2 layers due to the thermo-optic effect and a change in ambient humidity in the vicinity of the Bragg stack. Upon cooling the Bragg stack below RT, the RH close to the Bragg stack surface increases with respect to that of ambient air, leading to adsorption of water into the pores of the BS. Likewise, heating gives rise to desorption of
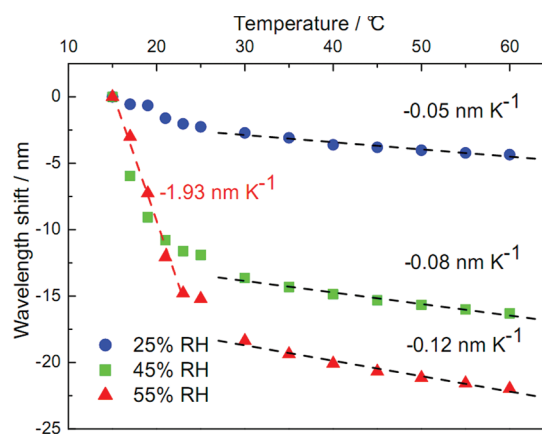

Figure 5. Wavelength shift as a function of temperature at different RHs. The shifts were obtained by extracting the wavelength values at 50% transmission from the spectra presented in Figure 3 for the temperatures between 15 and 60 °C at various RHs. The shifting behavior is strongly dependent on the RH. For temperatures above 30 °C the shift is linear. The linear approximation between 30 and 60 °C shows the rate of the shift being equal to -0.05, -0.09, and -0.12 nm K^{-1} for RHs 25%, 45%, and 55%, respectively. Below ≈ 30 °C we observe a nonlinear behavior of the shift, showing a higher slope of up to -1.93 nm K^{-1}.

water from the Bragg stack. The capillary system of the interparticle pores facilitates penetration of water into the whole volume of the photonic crystal and diffusion throughout the mesopore system.[34] As the BS is cooled down, the effective refractive index of the material increases due to water adsorption, thus shifting the position of the stop band to the red. We observed the wavelength shift without a change in the transmission profile and intensity, which indicates that the adsorption/desorption effect occurs in the entire multilayer[15] and that there are no scattering losses due to water condensation on the surface of the BS. However, the Bragg stack should not be cooled down to temperatures lower than the dew point for the corresponding relative humidity of the environment. We also analyzed the possible influence of the thermal expansion on the tuning properties of the BS. According to the literature, the thermal expansion coefficients of nanocrystalline anatase (crystallite size ≈ 9 nm) and of silicon dioxide in air are 8.57×10^{-6} and 0.50×10^{-6} K^{-1}, respectively.[35,36]
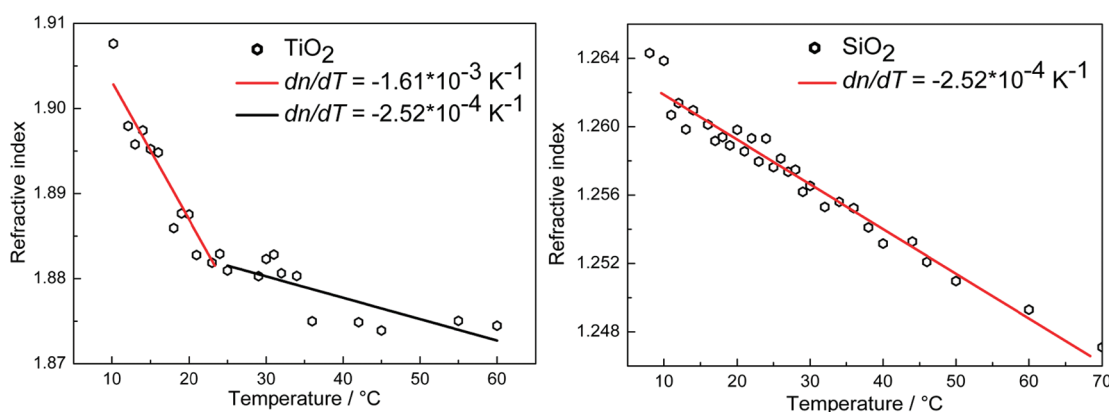
Figure 6. Dependence of the refractive index on the temperature for TiO_2 (66 nm) and SiO_2 (111 nm) single thin films measured by spectroscopic ellipsometry at RH 25%. The refractive index was determined at 530 nm.

Using the given values, the increase in thickness amounts to approximately 0.02 nm for the 60 nm TiO_2 and 93 nm SiO_2 films in the studied range from 15 to 60 °C. This value has negligible effect on the RI change and at the same time slightly shifts the stop band position to longer wavelengths at higher temperatures, i.e., contrary to the shift based on the TOC (Figure S3). We also investigated the behavior of the film thickness in situ at ambient conditions by means of spectroscopic ellipsometry to probe possible swelling of the inorganic layer due to water adsorption. According to the conducted measurements the thickness of the thin films does not change within the given temperature range, taking into account an error of 0.2 nm.

In order to support the argument of humidity-based amplification of the temperature response, optical spectra of the Bragg stack at different humidities were recorded at constant temperature (Figure 4). This experiment was designed to determine the pure humidity response of the BS. To this end, the measurement setup was supplemented by a tubing that guided humid air onto the sample, the RH of which was controlled by blowing it through a water-filled bubbler. The stop band of the Bragg stack shifted to the red by 11 nm after increasing the RH from 40% to 80% at RT without scattering losses in transmission. Repeated cycling between these two RHs was fully reversible. This observation is in accord with the fact that the transmission curves of the BS taken at the same temperature, but different RHs (Figure 3), are red-shifted with respect to each other upon increasing RH.

From Figure 5 it becomes evident that the temperature response is nonlinear; i.e., increasingly larger shifts are observed at lower temperatures. We rationalize this finding by enhanced water adsorption into the pores as the dew point is approached, which maps the exponential behavior of the RH as a function of temperature (Figure S4, see the Supporting Information for additional details). As the temperature is increased, water is increasingly desorbed from the pores such that above RT the shift is governed predominantly by the thermo-optic effect. We can therefore describe the thermal tuning of the Bragg stack as the superposition of the changes in temperature and the relative humidity during heating (cooling). The linear approximation of the temperature response in the range between 30 and 60 °C gives shifts of −0.05, −0.08, and −0.12 nm K^{-1} for 25%, 45%, and 55%, respectively. Below 30 °C we observe a nonlinear shift behavior, showing steeper slopes of the shifts at higher humidities. The humidity-enhanced thermal tuning causes shifts of the transmission spectra by up to −1.93 nm K^{-1} as compared to

0.35 nm K^{-1} calculated for typical nonporous Si/SiO_2 BSs.[37] The observed optical response thus correlates with the dependence of the humidity on temperature for various dew points (Figure S4). The dew points are 11 °C for ambient air at 55% RH, 7 °C for 45% RH, and 0 °C for 25% RH. Graph S4 evidences that the slope of the curves is significantly steeper below RT for all dew points and, notably, that upon temperature change from 20 to 10 °C the increase in humidity and hence optical shift is significantly larger for the 55% setting (dew point 11 °C) than for the 25% setting (dew point 0 °C), which corresponds well with our measurements.

In order to verify the experimental results, we carried out simulations of the transmission spectra with the program COMSOL Multiphysics 3.3 based on the experimental layer thicknesses and effective refractive indices of the respective layers.[38] To simulate the thermal behavior, the thermo-optic coefficients of TiO_2 and SiO_2 were required. Due to a lack of literature data on the TOC (dn/dT) for nanoparticle-based TiO_2 and SiO_2 films, we measured the dependence of the RI on temperature by spectroscopic ellipsometry at temperatures between 10 and 60 °C at 25% relative humidity (Figure 6). The acquired data were fitted to the Cauchy dispersion equation for the visible wavelength region. The RI was determined at 530 nm. We observed a linear behavior of RI for SiO_2 between ≈12 and 60 °C. The effective TOC was determined to be -2.52×10^{-4} K^{-1}. Thus, in contrast to the majority of literature sources that report positive TOC values for silicon dioxide, we measured a negative trend in the refractive index change as a function of temperature. However, Müller et al. also observed a negative TOC of -1.92×10^{-5} K^{-1} for SiO_2 in an intermediate buffer layer between Si substrate and metal oxide film and attributed such behavior to the difference in the TEC of the silicon substrate and amorphous silica.[39] According to the above-mentioned report, the temperature-induced extension of bulk silicon substrate causes stretching of the SiO_2 film, thus reducing the RI of the film. The TOC of SiO_2 determined in our study has a ~13 times higher value, which can be explained by the additional influence of the previously described humidity effect. The TiO_2 film shows a nonlinear $n(T)$ behavior which can be approximated by two separate negative slopes switching around 30 °C. The region between 10 and 30 °C is described by $dn/dT = -1.61 \times 10^{-3}$ K^{-1}, whereas above 30 °C a lower TOC of -2.52×10^{-4} K^{-1} was measured. We extracted the RIs corresponding to the respective temperatures and used them as input parameters for
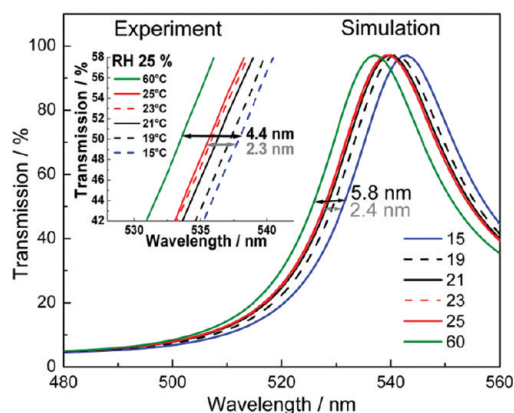
Figure 7. Correlation between the simulated and experimental transmission spectra at 25% RH. Simulations are based on the effective thermo-optic coefficients of the individual TiO$_2$ and SiO$_2$ layers determined by spectroscopic ellipsometry at 25% RH (see Figure 6).

the simulations. The simulations of the wavelength shift based on the *effective* TOCs for single TiO$_2$ and SiO$_2$ films at ambient conditions essentially reproduce the experimental values for the BSs measured at the same RH of 25% (Figure 7). The shift determined from the simulations is nonlinear and equal to 2.4 nm between 15 and 25 °C, which confirms the experimentally measured shift of 2.5 nm in the same temperature range. The overall shift of 5.8 nm between 15 and 60 °C is also in close agreement to the experimental value of 4.4 nm.

CONCLUSIONS

We have presented a comprehensive study of the oftentimes neglected influence of ambient conditions on the thermal tunability of nanoparticle-based one-dimensional TiO$_2$/SiO$_2$ photonic crystals. Reversible tuning was achieved through the thermo-optic effect in the Bragg stack layer materials. Due to the porous nature of the multilayer, we observe spectral shifts of different magnitude at various relative humidities. Notably, the shift is significantly enhanced with increasing relative humidity of the environment, thereby amplifying the thermal response and, thus, sensitivity of the Bragg stack. The observed shifts range between 4.4 and 21.9 nm between 25% and 55% RH in the temperature range 15–60 °C. The temperature response is nonlinear at low temperatures and high humidities, whereas it approaches a linear behavior at increasing temperature as the impact of humidity decreases. The tuning efficiency during heating varies from −0.05 nm K^{-1} at 25% RH and −0.12 nm K^{-1} at 55% RH between 25 and 60 °C up to −1.93 nm K^{-1} at 55% RH between 15 and 25 °C. We assume that at lower temperatures ($T < 30$ °C) the shifting behavior is governed by a combination of water adsorption/desorption processes and the thermo-optic effect, whereas at higher temperatures ($T > 30$ °C) the shift is dominated by the thermo-optic effect and, thus, is essentially linear.

In summary, the detailed knowledge about the interplay between temperature- and humidity-based effects on the structural color of PCs facilitates the design of future PC architectures exhibiting decoupled temperature or humidity response, or coupled and hence enhanced temperature–humidity response. Along these lines, bottom-up assembly employing spin-coating of sol–gel nanoparticle suspensions can provide an easy-to-fabricate

and low-cost route to creating highly responsive functional PCs with various degrees of porosity for further sensitivity enhancement.

METHODS

Preparation of TiO$_2$ and SiO$_2$ Suspensions. The suspension of TiO$_2$ nanoparticles was synthesized by the sol–gel hydrolysis of titanium(IV) ethoxide (6.25 mL, technical grade, Aldrich) in HNO$_3$ (0.1 M, 37.5 mL).[40] Titanium(IV) ethoxide was added dropwise to the acid at room temperature during vigorous stirring in a N$_2$ atmosphere. The mixture was then heated at 80 °C for 8 h. The subsequent sonication (Elmasonic S100/H, 37 kHz) of the sol allowed obtaining nanoparticles with a hydrodynamic diameter in the range between 7 and 15 nm. SiO$_2$ colloids (hydrodynamic diameter 6–10 nm) were purchased from Sigma-Aldrich (LUDOX SM-30, 30 wt % in H$_2$O) and diluted with distilled water using a ratio of 1:5. Particle size distribution of the precursor TiO$_2$ and SiO$_2$ suspensions was analyzed using dynamic light scattering photocorrelation spectroscopy (Malvern Nano ZS Zetasizer) at 20 °C. The crystalline nature of the TiO$_2$ powder calcined at 350 °C for 1 h was confirmed by X-ray diffraction (Bruker D8 Discover).

Bragg Stack Assembly. Thermoresponsive photonic crystals were assembled by sequential deposition of TiO$_2$ and SiO$_2$ suspensions on a clean ISO 8037/1 glass side (2.5 × 2.5 cm^2) previously activated by air plasma treatment (Femto, Diener Electronic). To improve the TiO$_2$ film quality, 2.5 wt % of poly(ethylene glycol) (PEG, M_w = 8000 g mol^{-1}) was added for spin coating. Both suspensions were filtered using syringe filters (SPARTAN 13, 0.2 μm) to remove aggregates. Thin layers of TiO$_2$ and SiO$_2$ were produced by using the spin-coating technique (Laurell WS-650SZ-6NPP/LITE). The glass slides were covered by 200–250 μL of TiO$_2$ suspension and accelerated at 1500 rpm s^{-1} to final rotation speeds ranging from 2500 to 5500 rpm. The total spin-coating process for each layer was completed in 60 s. Afterward the sample was put into a muffle furnace (Nabertherm, L3/11/B810) for calcination at 350 °C for 30 min. The same procedure was applied to the deposition of the following layers until 8.5 TiO$_2$/SiO$_2$ bilayers were assembled. The single thin film thickness was characterized by spectroscopic ellipsometry (performed on a Woollam M200D variable angle ellipsometer in the entire spectral range of 190–1000 nm at angles of incidence of 65°, 70°, 75°) and profilometry (Dektak-150 Stylus profiler BRUKER AXS). To investigate the porosity of the layers an ellipsometric porosimetry setup was used. The RIs of the SiO$_2$ and TiO$_2$ single films were measured first with void pores and then with the pores filled with toluene. Scanning electron microscopy (JEOL JSM-6500F operating at an accelerating voltage of 4 kV) was used to examine the morphology of the BS cross section.

Thermo-optical Analysis. To obtain transmission spectra of the Bragg stack in the range of 400–800 nm, we used a monochromator (Cornerstone260 1/4 m) with a high-pressure arc lamp as a light source and a 10 × 10 mm calibrated silicon detector connected to a digital lock-in amplifier (Merlin). The sample was mounted in the sample holder and placed before the detector in a closed chamber (the distances "monochromator-sample" and "sample-detector" were 8 and 12 cm, respectively). The temperature of the Bragg stack was varied by two Peltier elements that were placed onto the sample and arranged with a 4 mm gap in between to provide the optical axis. The PT100

303

dx.doi.org/10.1021/jp208733t | *J. Phys. Chem. C* 2012, 116, 298–305

temperature sensor was attached to the other side of the Bragg stack above the optical axis. Peltier elements and the temperature sensor were connected to a remote-controlled source meter. A software proportional integral controller regulated the heating and cooling of the Peltier elements. The measured deviation of the temperature during the measurement was less than 0.1 °C. For each temperature the sample was equilibrated for 60 s. We changed the relative humidity (RH) or the environment by introducing the water vapor into the monochromator chamber. The RH was varied between 25% and 80%. To measure the TOC of the TiO_2 and SiO_2 thin films, we used a heating stage (Peltier element) mounted into the house of the ellipsometer. The measurement was done when the sample was equilibrated at the desired temperature. The temperature was varied from 12 to 60 °C.

■ ASSOCIATED CONTENT

Ⓢ Supporting Information.   X-ray diffraction of TiO_2 powder; number-size distribution of TiO_2 and SiO_2 measured by dynamic light scattering; spectral shift; dependence of RH of air on temperature. This material is available free of charge via the Internet at http://pubs.acs.org.

■ AUTHOR INFORMATION

Corresponding Author
*E-mail bettina.lotsch@cup.uni-muenchen.de.

Author Contributions
⊥These authors contributed equally to this work.

■ ACKNOWLEDGMENT

■ REFERENCES

(1) Bechtold, T.; Rudnyi; E. B.; Korvink, J. G. *Fast Simulation of Electro-Thermal MEMS. Efficient Dynamic Compact Models*; Fujita, H., Liepmann, D. , Eds.; Springer−Verlag: Berlin, Heidelberg, Germany, 2007; pp 65−67.

(2) Yu, K.; Park, N. Characterization of MEMS Optical Bandpass Filters with Narrow Transition Bands. *Proc. SPIE—Int. Soc. Opt. Eng.* **2005**, *6021*, 60212R.

(3) Lammel, G.; Schweizer, S.; Renaud, P. Microspectrometer Based on a Tunable Optical Filter of Porous Silicon. *14th IEEE Int. Conf. MEMS* **2001**, 578−81.

(4) Ge, J.; Yin, Y. Responsive Photonic Crystals. *Angew. Chem., Int. Ed.* **2011**, *50*, 1492−1522.

(5) Nair, R. V.; Vijaya, R. Photonic Crystal Sensors: An Overview. *Prog. Quant. Electron.* **2010**, *34*, 89−134.

(6) Joannopoulos, J. D.; Johnson, S. G.; Winn, J. N.; Meade, R. D. *Photonic crystals: Molding the flow of light*, 2nd ed.; Princeton University Press: Princeton, NJ, 2008; pp 44−65.

(7) Bonifacio, L. D.; Lotsch, B. V.; Puzzo, D. P.; Scotognella, F.; Ozin, G. A. Stacking the Nanochemistry Deck: Structural Diversity in One-Dimensional Photonic Crystals. *Adv. Mater.* **2009**, *21*, 1641−1646.

(8) Gülşen, G.; Inci, M. N. Thermal Optical Properties of TiO_2 Films. *Opt. Mater.* **2002**, *18*, 373−381.

(9) Xie, H; Ng, F. L.; Zeng, X. T. Spectroscopic Ellipsometry Study of Thin Film Thermo-Optical Properties. *Thin Solid Films* **2009**, *517*, 5066−5069.

(10) Ghosh, G. Model for the Thermo-Optic Coefficients of Some Standard Optical Glasses. *Non-Cryst. J. Solids* **1995**, *189*, 191−196.

(11) Hohlfeld, D.; Zappe, H. An All-Dielectric Tunable Optical Filter Based on the Thermo-Optic Effect. *J. Opt. Soc. Am. A: Pure Appl. Opt.* **2004**, *6*, 504−511.

(12) Hohlfeld, D.; Epmeier, M.; Zappe, H. A Thermally Tunable, Silicon Based Optical Filter. *Sens. Actuators, A* **2003**, *103*, 93−99.

(13) Regoliosi, P.; Guehl, M.; Scarpa, G.; Lugli, P.; Persano, L.; Del Carro, P.; Camposeo, A.; Cingolani, R.; Pisignano, D.; Bietti, S.; et al. Thermal Tunability of Monolithic Polymer Microcavities. *Appl. Phys. Lett.* **2008**, *92*, 253−310.

(14) Beregovski, Y.; Hennig, O.; Fallahi, M.; Guzman, F.; Clemens, R.; Mendes, S.; Peyghambarian, N. Design and Characteristics of DBR-Laser-Based Environmental Sensors. *Sens. Actuators, B* **1998**, *53*, 116−124.

(15) Pellicori, S. F.; Hettich, H. L. Reversible Spectral Shift in Coatings. *Appl. Opt.* **1988**, *27*, 3061−3062.

(16) Saxe, S. G.; Messerly, M. J.; Bovard, B.; DeSandre, L.; Van Milligen, F. J.; Macleod, H. A. Ion Bombardment-Induced Retarded Moisture Adsorption in Optical Thin Films. *Appl. Opt.* **1984**, *23*, 3633−3637.

(17) Hirsch, E. H. Stress in Porous Thin Films through Adsorption of Polar Molecules. *J. Phys. D: Appl. Phys* **1980**, *13*, 2081−2094.

(18) Macleod, H. A.; Richmond, D. Moisture Penetration Patterns in Thin Films. *Thin Solid Films* **1976**, *37*, 163−169.

(19) Pulker, H. K. Characterization of Optical Thin Films. *Appl. Opt.* **1979**, *18*, 1969−1977.

(20) Gibson, D. R; Lissberger, P. H. Optical Properties of Narrowband Spectral Filter Coatings Related to Layer Structure and Preparation. *Appl. Opt.* **1983**, *22*, 269−281.

(21) Brunsting, A.; Kheiri, M. A.; Simonaitis, D. F.; Dosmann, A. J. Environmental Effects on All-Dielectric Bandpass Filters. *Appl. Opt.* **1986**, *25*, 3235−3241.

(22) Colodrero, S.; Ocana, M.; Míguez, H. Nanoparticle-Based One-Dimensional Photonic Crystals. *Langmuir* **2008**, *24*, 4430−4434.

(23) Chen, K. M.; Sparks, A. W.; Luan, H. C.; Lim, D. R.; Wada, K.; Kimerlinga, L. C. SiO_2/TiO_2 Omnidirectional Reflector and Microcavity Resonator via the Sol-Gel Method. *Appl. Phys. Lett.* **1999**, *75*, 3805−3807.

(24) Choi, S. Y.; Mamak, M.; von Freymann, G.; Chopra, N.; Ozin, G. A. Mesoporous Bragg Stack Color Tunable Sensors. *Nano Lett.* **2006**, *6*, 2456−2461.

(25) Kobler, J.; Lotsch, B. V.; Ozin, G. A.; Bein, T. Vapor-Sensitive Bragg Mirrors and Optical Isotherms from Mesoporous Nanoparticle Suspensions. *ACS Nano* **2009**, *3*, 1669−1676.

(26) Lee, D.; Rubner, M. F.; Cohen, R. E. All-Nanoparticle Thin-Film Coatings. *Nano Lett.* **2006**, *6*, 2305−2312.

(27) Colodrero, S.; Ocaña, M.; Gonzailez-Elipe, A. R.; Míguez, H. Response of Nanoparticle-Based One-Dimensional Photonic Crystals to Ambient Vapor Pressure. *Langmuir* **2008**, *24*, 9135−9139.

(28) Calvo, M. E.; Colodrero, S; Rojas, C. T.; Ocaña, M.; Anta, J. A.; Míguez, H. Photoconducting Bragg Mirrors Based on TiO_2 Nanoparticle Multilayers. *Adv. Funct. Mater* **2008**, *18*, 2708−2715.

(29) Fuertes, M. C.; Colodrero, S.; Lozano, G.; Gonzalez-Elipe, A. R.; Grosso, D.; Boissiere, C.; Sanchez, C.; Soler-Illia, G. J. A. A.; Míguez, H. Sorption Properties of Mesoporous Multilayer Thin Films. *J. Phys. Chem. C* **2008**, *112*, 3157−3163.

(30) Fuertes, M. C.; Lopez−Alcaraz, F. J.; Marchi, M. C.; Troiani, H. E.; Luca, V.; Míguez, H.; Soler-Illia, G. J. A. A. Photonic Crystals from Ordered Mesoporous Thin-Film Functional Building Blocks. *Adv. Funct. Mater.* **2007**, *17*, 1247−1254.

(31) Wu, Z.; Lee, D.; Rubner, M.; Cohen, R. E. Structural Color in Porous, Superhydrophilic, and Self-Cleaning SiO_2/TiO_2 Bragg Stacks. *Small* **2007**, *3*, 1445−1451.

(32) Baklanov, M. R.; Mogilnikov, K. P. Non-Destructive Characterisation of Porous Low-k Dielectric Films. *Microelectron. Eng.* **2002**, *64*, 335−349.

(33) Eslava, S.; Baklanov, M. R.; Kirschhock, C. E. A.; Iacopi, F.; Aldea, S.; Maex, K.; Martens, J. A. Characterization of a Molecular Sieve Coating Using Ellipsometric Porosimetry. *Langmuir* **2007**, *23*, 12811–12816.

(34) Puzzo, D. P.; Bonifacio, L. D.; Oreopoulos, J.; Yip, C. M.; Manners, I.; Ozin, G. A. Color from Colorless Nanomaterials: Bragg Reflectors Made of Nanoparticles. *J. Mater. Chem.* **2009**, *19*, 3500–3506.

(35) Jagtap, N.; Bhagwat, M.; Awati, P.; Ramaswamy, V. Characterization of Nanocrystalline Anatase Titania: An *in Situ* HTXRD Study. *Thermochim. Acta* **2005**, *427*, 37–41.

(36) Tada, H.; Kumpel, A. E.; Lathrop, R. E.; Slanina, J. B.; Nieva, P.; Zavracky, P.; Miaoulis, I. N.; Wong, P. Y. Thermal Expansion Coefficient of Polycrystalline Silicon and Silicon Dioxide Thin Films at High Temperatures. *J. Appl. Phys.* **2000**, *87*, 4189–4193.

(37) Banerjee, A. Enhanced Temperature Sensing by Using One-Dimensional Ternary Photonic Band Gap Structures. *PIER Lett.* **2009**, *11*, 129–137.

(38) The COMSOL *Multiphysics* Version 3.3 simulation software: http://www.comsol.com/.

(39) Wiechmann, S.; Müller, J. Thermo-Optic Properties of TiO_2, Ta_2O_5 and Al_2O_3 Thin Films for Integrated Optics on Silicon. *Thin Solid Films* **2009**, *517*, 6847–6849.

(40) Lotsch, B. V.; Ozin, G. A. Photonic Clays: A New Family of Functional 1D Photonic Crystals. *ACS Nano* **2008**, *2*, 2065–2074.